

## Adhesion and reliability of copper interconnects with Ta and TaN barrier layers

Michael Lane and Reinhold H. Dauskardt

*Department of Materials Science and Engineering, Stanford University,  
Stanford, California 94305-2205*

Nety Krishna and Imran Hashim

*Applied Materials Corporation, Santa Clara, California 95052*

(Received 20 August 1999; accepted 25 October 1999)

With the advent of copper metallization in interconnect structures, new barrier layers are required to prevent copper diffusion into adjacent dielectrics and the underlying silicon. The barrier must also provide adequate adhesion to both the dielectric and copper. While Ta and TaN barrier layers have been incorporated for these purposes in copper metallization schemes, little quantitative data exist on their adhesive properties. In this study, the critical interface fracture energy and the subcritical debonding behavior of ion-metal-plasma sputtered Ta and TaN barrier layers in Cu interconnect structures were investigated. Specifically, the effects of interfacial chemistry, Cu layer thickness, and oxide type were examined. Behavior is rationalized in terms of relevant reactions at the barrier/dielectric interface and plasticity in adjacent metal layers.

### I. INTRODUCTION

Current semiconductor technology dictates the use of low-resistivity metal lines for multilayer interconnect devices. Currently, Al–Cu metal layers are employed in most devices; however, copper has emerged as an attractive alternative. Copper has a higher conductivity and superior electromigration resistance than aluminum alloys leading to shorter resistance capacitance (RC) delay times and reduced failure due to electromigration.<sup>1–3</sup> However, integration of Cu lines into interconnect structures poses several challenges. Cu is a more mobile element than Al and, for example, diffuses rapidly in SiO<sub>2</sub> and forms silicides at temperatures as low as 200 °C.<sup>1,4,5</sup> A reliable barrier layer is therefore needed to inhibit the diffusion of copper into adjacent dielectric layers and the silicon substrate. In addition, the barrier layer must also provide adequate adhesion to both the dielectric and metal layers. The resulting adhesive strength must be able to withstand the high residual stresses associated with thermal expansion mismatch and film growth processes, as well as the high back stresses developed during electromigration processes in the Cu lines.<sup>2,3</sup>

Tantalum and tantalum-based films have emerged as promising diffusion barriers for copper interconnects. While much effort has been made to characterize the phase stability and diffusion barrier properties of these layers (e.g., Refs. 6 and 7), almost no attention has been given

to their adhesive and fracture properties. Accordingly, in this study we address the adhesion and subcritical debonding behavior of the barrier/SiO<sub>2</sub> interface, together with its microstructural and chemical determinants.

By adhesion we are primarily concerned with the total energy required to separate an interface, measured in terms of a critical value of the debond strain energy release rate or interface debond energy,  $G_c$  (J/m<sup>2</sup>).<sup>8</sup> This energy includes not only the breaking of chemical bonds across the interface but also plasticity in any adjacent ductile layers. Energy dissipation in debond wake processes (such as a frictional contact zone) must also be considered. Previous work has shown that each of these processes can significantly affect the critical interface debond energy.<sup>9–12</sup> In the case of Al–Cu interconnects, plastic dissipation in the metal layer adjacent to the interface of interest was found to increase the interface fracture energy by over 300% when the Al–Cu layer thickness was increased from 0.1 to 4.0 μm.<sup>9–11</sup> Likewise, increasing the roughness of the interface was found to increase interface fracture energies by 25% for root-mean-square (rms) roughness changes of as little as 7%.<sup>12</sup> These energy-dissipation processes typically do not act independently but behave in a synergistic fashion. In addition, both processes of frictional contact and plasticity scale with the interfacial chemical bond strength so that moderate changes in interfacial chemistry may have pronounced effects on the macroscopic work of adhesion.<sup>8,11,13–15</sup>

Of equal importance is the phenomenon of subcritical debonding which may lead to time-dependent failure of device structures either during fabrication or in service.<sup>9,11,16,17</sup> Preexisting flaws at an interface may grow subcritically over time at a strain energy release rate,  $G$ , far lower than the critical interface debond energy,  $G_c$ . Previous work on Al–Cu interconnect structures has shown that strain energy release rates of less than 50% of  $G_c$  may propagate debonds along an interface.<sup>9,11</sup> Furthermore, environmental factors such as moisture content and temperature may significantly accelerate the debond growth velocity. The mechanical driving forces for such time-dependent delamination processes include residual thermal expansion mismatch and growth stresses, alternating stresses from thermal cycling, and electromigration back-stresses. During fabrication the mechanical stresses and moist environments associated with chemical mechanical processing (CMP) operations may be particularly deleterious.

The objective of this paper is therefore to report on progress toward characterizing and understanding the adhesion in interconnect structures employing copper metallization and a selected range of adjacent barrier and dielectric layers. Specifically, issues of plasticity in the copper layer, type of dielectric oxide, and barrier layer chemistry are investigated. Adhesion and subcritical debonding data are presented for a selected range of Ta and TaN barrier layers. The presence of N in the barrier layer is shown to significantly improve adhesion and resistance to subcritical debonding. Behavior is rationalized in terms of relevant reactions at the barrier/SiO<sub>2</sub> interface and plasticity in the adjacent copper layer.

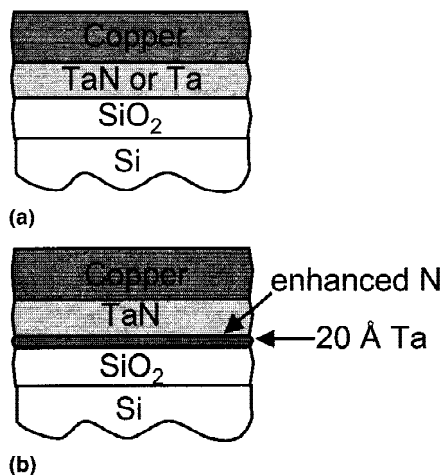
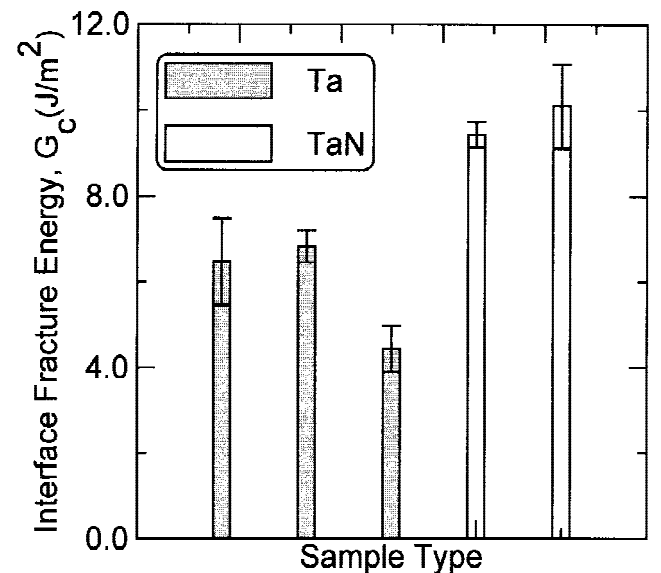


FIG. 1. Schematic illustration of the thin-film structures with Cu metallization showing (a) TaN or Ta barrier layers and (b) the TaN/Ta barrier stack.

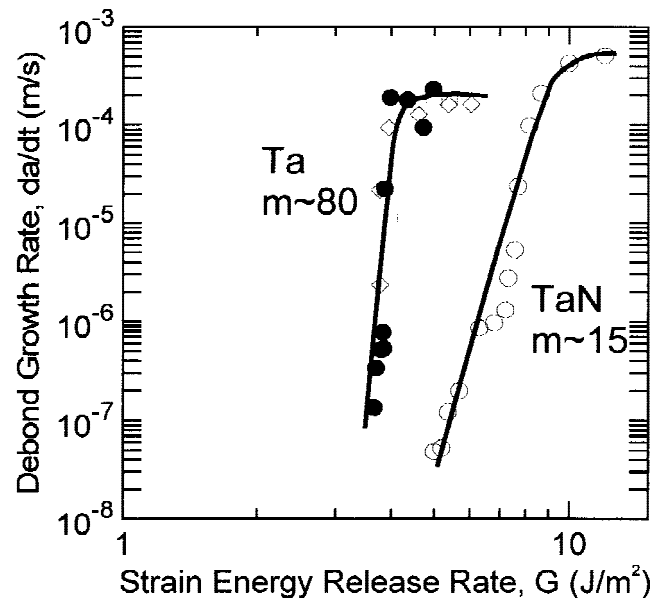
## II. EXPERIMENTAL PROCEDURES

### A. Sample preparation

Thin film stacks shown schematically in Fig. 1 were fabricated on 8-in. silicon wafers using ion-metal-plasma sputtering (for metal and barrier layers) on thermal oxide. One sample set was fabricated with the above stack structure on tetraethyl orthosilicate (TEOS) oxide in order to assess the effects of oxide type. Nominal thickness for the Ta and TaN layers were 250 Å, with 1500 Å for the Cu layer. The TaN layer was deposited by sputtering Ta while flowing N<sub>2</sub> into the chamber resulting in a uniform



(a)



(b)

FIG. 2. Effect of Ta and TaN barrier layers on (a) the barrier layer/SiO<sub>2</sub> interface adhesion and (b) the subcritical debond growth rate as a function of the debond strain energy release rate,  $G$ .

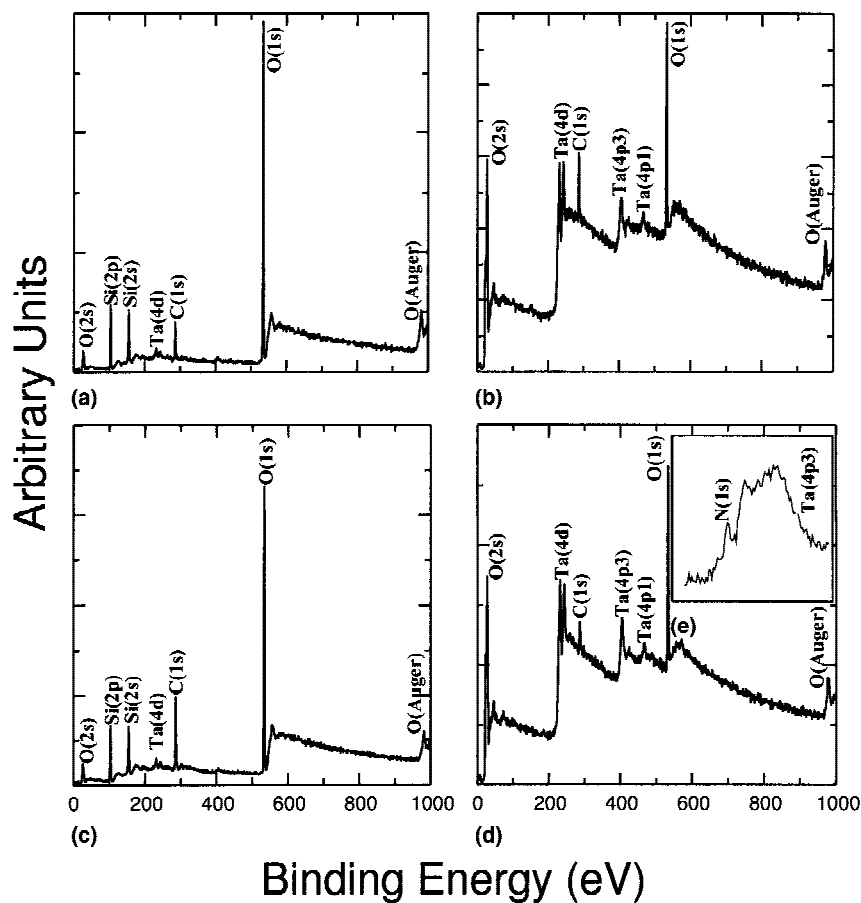


FIG. 3. XPS spectra obtained from fracture surfaces of samples with the Ta barrier layer showing (a) the SiO<sub>2</sub> side and (b) the Ta side, samples with TaN barrier layers showing (c) the SiO<sub>2</sub> side and (d) the TaN side, and (e) a detailed scan showing N and Ta on the SiO<sub>2</sub> side of the fracture surface.

TaN layer with 30 at.% N, which lies in the Ta<sub>2</sub>N region of the equilibrium phase diagram [Fig. 1(a)]. Additional TaN/Ta(N)/SiO<sub>2</sub> samples were fabricated by first depositing a 20 Å Ta layer and subsequently depositing the TaN layer [Fig. 1(b)]. The initial N<sub>2</sub> flow was altered so as to produce films with ~30, 40, and 50 at.% N at the Ta(N)/SiO<sub>2</sub> interface as measured by Rutherford backscattering spectroscopy (RBS). However, the resulting N enhancement was only in the first few angstroms adjacent to the Ta(N)/SiO<sub>2</sub> interface and the TaN film retained desirable properties for semiconductor metallization. Physical vapor deposition (PVD) processing by first depositing 20 Å of Ta and then flowing N<sub>2</sub> into the chamber for subsequent deposition of the layer assisted in keeping the Ta source free of TaN contamination. These samples were also fabricated without the Cu layer and heat treated to simulate subsequent sample preparation procedures in order to facilitate chemical analysis of the interface and the TaN films. A thicker Cu layer of 1.65 μm was also produced using electroplating in order to determine the effects of metal layer thickness.

## B. Adhesion and subcritical debonding tests

The thin-film stack of interest was sandwiched between two elastic silicon substrates in order to fabricate four-point flexure samples for adhesion testing.<sup>9,11</sup> As debonding occurs in these sandwiched configurations, the films of interest are constrained by the adjacent silicon substrate and adhesion values are not affected by relaxation of residual film stresses.<sup>11</sup> Two 35 × 35 mm squares were cleaved from each wafer and diffusion bonded at 400 °C for 4 h at a pressure of 12 MPa in a vacuum press. The squares were then diced into strips ~3 mm wide using a high-speed diamond saw. A notch was machined through the top Si wafer to within ~20 μm of the interface to initiate debonding. The side faces of some samples were polished with an aluminum slurry to facilitate *in situ* viewing of the debond process and inhibit fracture of the Si substrate during testing. The four-point flexure samples were tested in a high-stiffness micromechanical test system with fully articulating four-point bending fixtures employing a piezoelectric actuator. The samples were loaded at a displacement rate of

TABLE I. Properties of various glasses taken from Ref. 21.

	Soda lime	Borosilicate	Oxynitride
Density, $\rho$	2.47	2.23	3.8
Elastic Modulus, $E$ (GPa)	68.9	64	154
Hardness, $H$ (GPa)	5.6	5.8	10.7
Toughness, $K_c$ (MPa m <sup>1/2</sup> )	0.77	0.76	0.97
Stress corrosion, $K_{TH}$ (MPa m <sup>1/2</sup> )	0.22	0.34	0.5

0.3  $\mu\text{m/s}$ , and loads were measured to a resolution of 0.01 N. Critical loads were taken from the plateau of the load–displacement curves. Plateau lengths were generally quite long and associated with several mm of debond extension. Eight to ten tests were conducted for each sample type. Subcritical debonding tests were facilitated by loading the sample to a predetermined load and then fixing the displacement. The general method has been described previously.<sup>11</sup> Tests were conducted in a laboratory air environment [relative humidity (RH)  $\sim$  45%] and at 25 °C. Several millimeters of debond extension were observed during the tests.

### C. X-ray photoelectron spectroscopy analysis

X-ray photoelectron spectroscopy (XPS) scans were made on mating fracture surfaces of failed samples. The surfaces were characterized using a Surface Science XPS unit with monochromatized Al  $K_{\alpha}$  x-ray radiation with an electron escape depth of  $\sim$ 20 Å. In order to characterize interface reaction products, a broad XPS (0–550 eV) scan was made of each mating fracture surface. Detailed scans were then made in regions of the spectra containing peaks of interest (O, Si, N, and Ta). Finally, samples nominally identical to the nitrogen-containing samples but processed without the copper layer were examined. Scans were made in the TaN film, at the interface and in the silica.

## III. RESULTS AND DISCUSSION

Interface adhesion values derived from plateaus on the load–displacement curves for different Cu/barrier layer/SiO<sub>2</sub> (thermal) systems are shown in Fig. 2(a). Error bars in the figure represent the scatter obtained from 8 to 10 measurements. Variation in the measured adhesion values for the different sample sets is attributed to interface chemistry variation from different deposition tools used in the study. The uniform TaN barrier layer was found to produce approximately twice the interfacial debond energy compared to the Ta barrier layer. Subcritical debonding data for these systems are presented in Fig. 2(b). The TaN/SiO<sub>2</sub> interface was found to be more resistant to subcritical debonding than the Ta/SiO<sub>2</sub> system as evidenced by the lower growth rates at a given strain energy release rate,  $G$ . Furthermore, there is a sig-

nificant difference in slope,  $m$ , of the two curves. The slope of the debond growth rate curve for the TaN/SiO<sub>2</sub> interface is similar to that reported for moisture assisted cracking of bulk SiO<sub>2</sub> glasses<sup>18</sup> and previously reported values for TiN/SiO<sub>2</sub> interfaces in similar interconnect structures.<sup>9,11,16,17</sup> In contrast, the slope of the Ta/SiO<sub>2</sub> interface debond growth rate versus strain energy release rate curve is very steep, much like that expected for the onset of threshold growth rate behavior where water molecules are sterically hindered from reaching the debond tip.<sup>19</sup> Further evidence of this phenomenon has been observed over a much wider range of temperatures and moisture contents, and a detailed model will be presented elsewhere.<sup>20</sup>

XPS scans of the resulting fracture surfaces [Figs. 3(a)–3(e)] clearly reveal that debonding is nominally along the barrier/SiO<sub>2</sub> interface rather than the barrier/Cu interface. Indeed, debonding of the barrier/Cu interface was never observed for the present sample sets. A detailed scan centered on the binding energy for N obtained from the SiO<sub>2</sub> side of the TaN barrier layer samples reveals the presence of N [Fig. 3(e)]. The presence of N on the SiO<sub>2</sub> fracture surface indicates that N does diffuse into the SiO<sub>2</sub> and suggests that guidance for understanding the increased adhesion for the TaN/SiO<sub>2</sub> interface over Ta/SiO<sub>2</sub> might be taken from the bulk glass literature. In general, N-containing glasses exhibit improved mechanical properties including increased toughness and subcritical crack-growth resistance over SiO<sub>2</sub> glasses (Table I).<sup>21,22</sup> The increase in toughness has been attributed to the replacement of bivalent O with trivalent N leading to a more cross-linked, mechan-

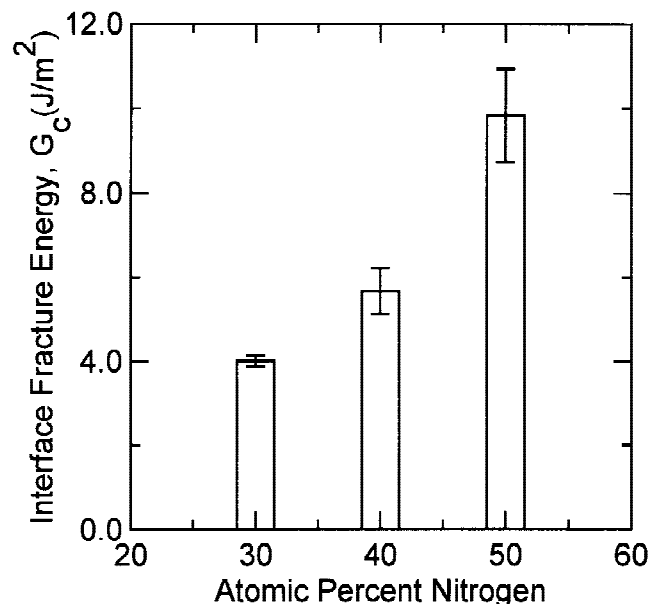


FIG. 4. Interface fracture energy as a function of nitrogen content at the Ta/SiO<sub>2</sub> interface in the TaN/Ta(N)/SiO<sub>2</sub> samples.

ically and chemically durable glass network structure.<sup>21</sup> The increased interface fracture resistance of TaN/SiO<sub>2</sub> over Ta/SiO<sub>2</sub> and the presence of N at the fracture surface in the TaN system indicates that a similar mechanism may be occurring, as discussed in more detail below.

The interface debond energy as a function of N content at the Ta(N)/SiO<sub>2</sub> interface in the TaN/Ta(N)/SiO<sub>2</sub> system is shown in Fig. 4. Interface fracture energy initially decreases from ~10 J/m<sup>2</sup> for the uniform TaN<sub>x</sub> layer to ~4 J/m<sup>2</sup> for samples produced with 30 at.% N at the interface. However, increasing the N content above 30 at.% at the Ta(N)/SiO<sub>2</sub> interface clearly increases the interface fracture energy. Specifically, increasing the N content by 10% (30 to 40 at.%) results in a 40% increase in interface fracture energy while increasing the N content by 20% (30 to 50 at.%) results in an increase in interface fracture energy of 145%. Indeed, samples with 50 at.% N exhibit fracture energies similar to samples processed with uniform TaN<sub>x</sub> compositions [Fig. 2(a)]. As previously noted, the interface chemistry is expected to significantly effect the overall debond energy since most energy absorbing processes scale with the work of adhesion.<sup>14,15</sup>

XPS analysis of the resulting fracture surfaces reveals two distinct fracture paths. Both the samples containing 30 and 40 at.% interfacial N fail nominally along the Ta(N)/SiO<sub>2</sub> interface similar to the Ta/SiO<sub>2</sub> samples, while the 50 at.% N samples failed in the SiO<sub>2</sub>. Representative scans for the 30 and 40 at.% samples are shown in Figs. 5(a) and 5(b). In both samples, ~2–3 at.% Si is observed on the Ta(N) fracture surface and approximately the same percentage of Ta is found on the SiO<sub>2</sub> side, again similar to the Ta/SiO<sub>2</sub> interface. Evidence of interfacial reactions was observed in both samples as illustrated by an asymmetric Si peak on the SiO<sub>2</sub> fracture surfaces and split Ta peaks on the Ta(N) side. The asymmetric Si peak and the split Ta peak correspond to different bonding states of Si and Ta, respectively. The ratio of the split peak heights changes as the N content is increased indicating that the amount of N present at the interface may play a role in determining the extent of interfacial reactions. A detailed analysis of the 50 at.% N-containing sample shows one side (SiO<sub>2</sub> side) with no measurable Ta signal but a robust N peak (~5 at.%), while the other side [Ta(N) side] has both Ta and N present in small amounts [Figs. 5(c) and 5(d)].

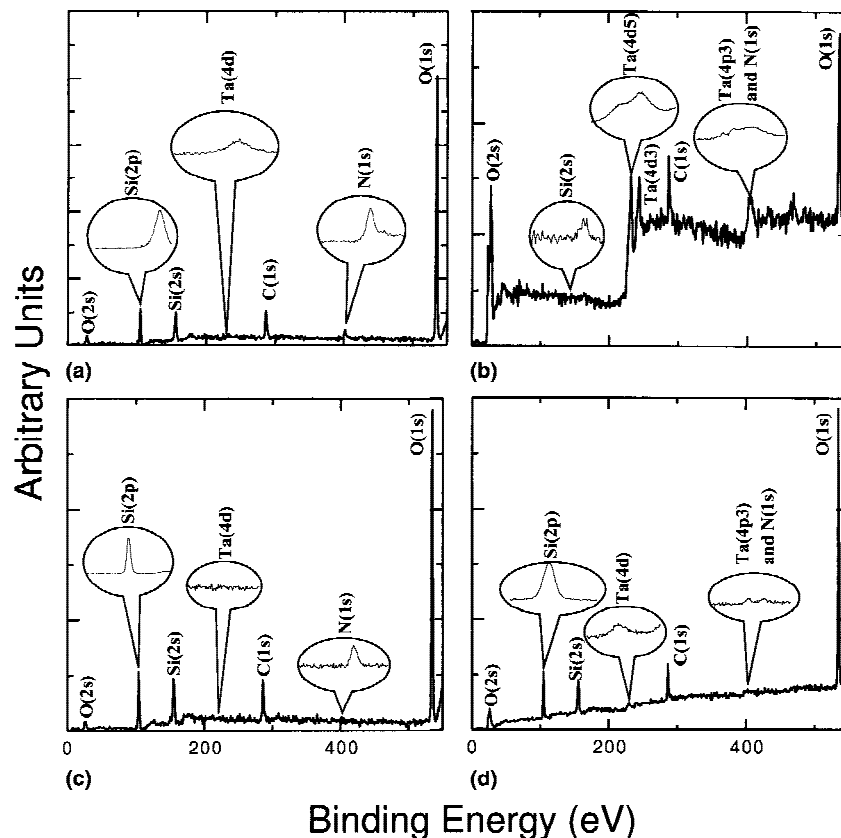


FIG. 5. Representative XPS results from the fractured specimens for the 30 and 40 at.% nitrogen samples showing (a) the SiO<sub>2</sub> side and (b) the Ta(N) side and results for the 50 at.% nitrogen samples showing (c) the SiO<sub>2</sub> side and (d) the Ta(N) side.

Before detailed consideration of the XPS results described above it should be noted that since the fractured samples were exposed to air, any elemental Ta present at the fracture surface would be expected to oxidize according to



where the enthalpy of formation determined from heats of formation of reactants under standard temperature and pressure conditions are shown to the right of the reaction.<sup>23</sup> Therefore, making direct inferences from the XPS data based on splits in the Ta peak for fracture paths exposed to the environment may be compromised.

As a first step toward addressing this issue and identifying interfacial reaction products, samples were examined with depth-profiling XPS. First, approximately 100 Å of the top TaN film was sputter etched away and scans were made of Ta, Si, N, and O peaks to establish a baseline for the TaN film. After scanning of the bulk TaN film, the remainder of the film was slowly sputter-etched away until a Si peak was observed indicating the presence of the Ta(N)/SiO<sub>2</sub> interface. Scans were taken of the same peaks as in the bulk. Representative results for the 50 at.% N-containing sample are summarized in Fig. 6.

Scans of the 30 and 40 at.% N samples were similar and differed only in the relative areas of the peaks which indicates different amounts of each bond type. Assignments of the various peaks can be made on the basis of literature values of binding energies as summarized in Table II. In particular, Ta<sub>2</sub>O<sub>5</sub> is indicated by the split Ta(4f<sub>7</sub>) peak and the tail on the low binding energy side of the asymmetric O(1s) peak while Ta<sub>2</sub>Si is also indicated by the split Ta(4f<sub>7</sub>) peak and the small Si(1s) peak at ~99 eV. The percent of elements in reaction products (TaO<sub>x</sub>, TaSi<sub>y</sub>, and SiN<sub>z</sub>) was found to increase as the nitrogen content at the interface was increased (Fig. 7). A schematic of the stack structure summarizing reaction layers and fracture paths is shown in Fig. 8.

On the basis of above results, it is possible to speculate on reactions that might take place at the oxide/barrier interface. Reactions to consider include oxidation of Ta, TaN, or Ta<sub>2</sub>N by SiO<sub>2</sub> according to

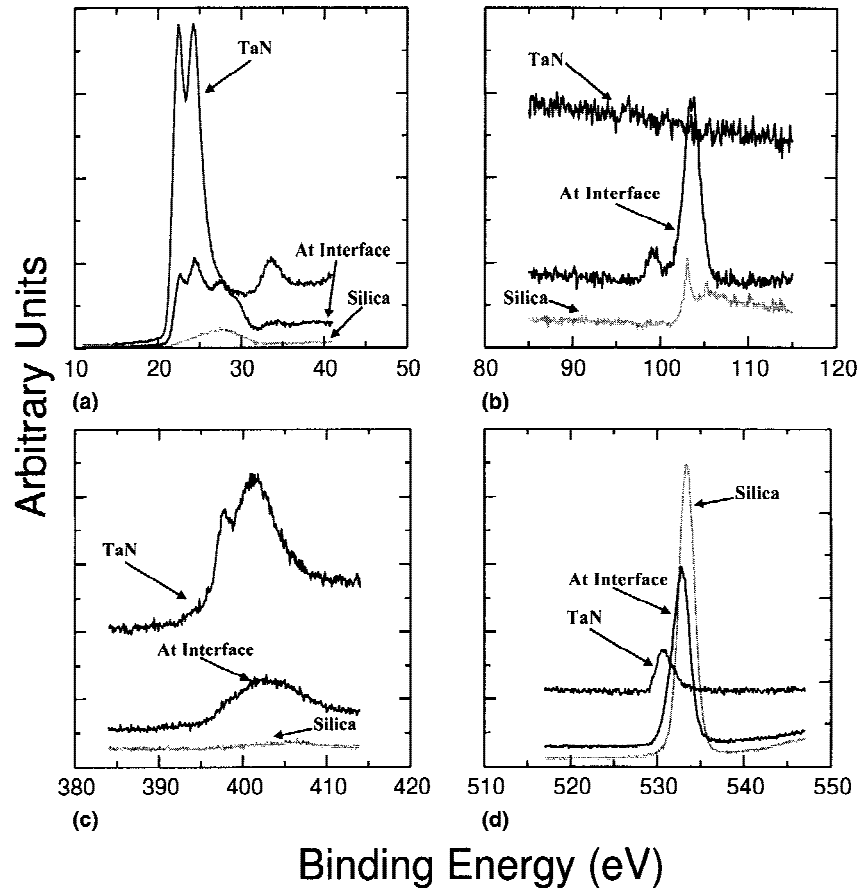
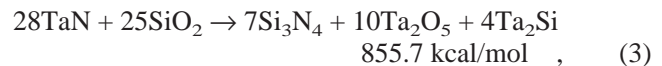
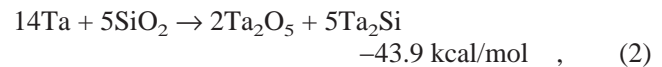
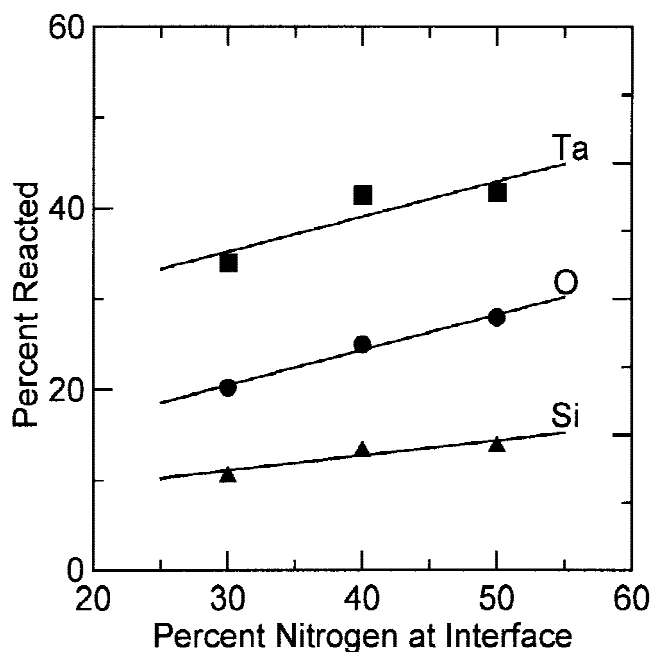
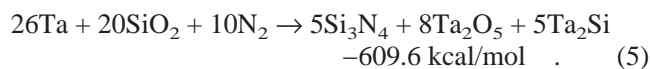
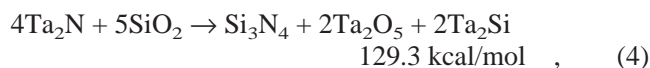


FIG. 6. Depth-profiling XPS scans taken at different locations for the 50 at.% nitrogen sample showing peaks for (a) Ta, (b) Si, (c) N, and (d) O.

TABLE II. Photoelectron peak binding energies taken from Ref. 28.

	Ta(4f7) (eV)	Si(1s) (eV)	O(1s) (eV)	N(1s) (eV)
Ta <sub>2</sub> O <sub>5</sub>	26.5–26.9	...	530.6	...
Ta <sub>2</sub> Si	27.0	99.4–100.5	...	...
SiO <sub>2</sub>	...	102.0–102.7	532.5–534.5	...
Ta	21.8	...	...	...
Si <sub>3</sub> N <sub>4</sub>	...	101.4–101.9	...	397.4–398.0

FIG. 7. Percent of reacted elements (TaO<sub>x</sub>, TaSi<sub>y</sub>, and SiN<sub>z</sub>) as a function of nitrogen content at the Ta(N)/SiO<sub>2</sub> interface in the TaN/Ta(N)/SiO<sub>2</sub> samples.

From a thermodynamic viewpoint, interfacial reactions will only occur if elemental Ta is present. For samples processed with a uniform TaN layer, initial processing involves the simultaneous deposition of elemental Ta and N, favoring reaction (5). Samples processed with a thin layer (~20 Å) of Ta before N<sub>2</sub> was introduced into the deposition chamber would initially favor reaction (2). However, with increasing N levels adjacent to the Ta layer, resulting diffusion of N to the interface accommodates reaction (5). It is not expected that the initial Ta layer is fully converted to TaN or Ta<sub>2</sub>N as reactions of those films with SiO<sub>2</sub> are not thermodynamically favorable [reactions (3) and (4)] and would not account for the observed decreases in TaN<sub>x</sub> and increase in adhesion as discussed below. Note also that although Si<sub>3</sub>N<sub>4</sub> was not directly observed in the depth-profiling experiment due

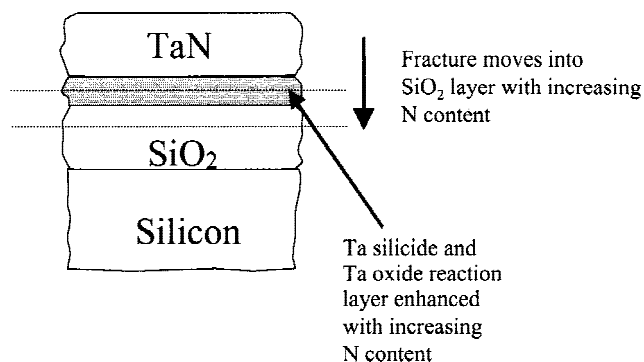


FIG. 8. Schematic of interface chemistry interpreted from XPS studies along with fracture path selection based on interfacial N content.

to the difficulty in separating the Ta(4p3) and N(1s) peaks, strong evidence of an oxynitride was observed as shown by Fig. 5(c) where a robust N peak is found on the SiO<sub>2</sub> fracture surface.

On the basis of reaction (5), as nitrogen diffuses to the interface the reaction enthalpy drops significantly (while N<sub>2</sub> may not be present at the interface, elemental N would make the reaction even more exothermic). From a chemical bonding viewpoint, an interface with a more negative reaction enthalpy is expected to have better adhesion than one with a more positive reaction enthalpy. This expectation, however, is predicated on the assumption that the interfacial reaction products are fracture resistant. Also, N is likely to be the limiting reagent in reaction (5) as it must diffuse through the thin Ta layer before the reaction may proceed. Note that the formation of Ta<sub>2</sub>N from Ta and N<sub>2</sub> is also a thermodynamically favorable reaction (-130 kcal/mol) and is expected to compete with the formation of the other reaction products. However, reaction (5) remains the dominant reaction, and the amount of Ta<sub>2</sub>N at the interface decreases with increasing N content as evidenced by Fig. 7, where the amount of reacted products (TaO<sub>x</sub>, TaSi<sub>y</sub>, and SiN<sub>z</sub>) increases with increasing N. We conclude that increasing the atomic concentration of N at the interface drives the reaction to the right resulting in increased reaction products. Further, the presence of N in the SiO<sub>2</sub> suggests the possibility of the formation of an oxynitride glass which is more fracture resistant. These two effects contribute to the improved interfacial adhesion as observed experimentally.

While changing the type of barrier layer in a copper interconnect structure clearly has a profound impact on the interface fracture energy, changing the oxide type also has a significant effect as shown in Fig. 9. Approximately 40% higher adhesion values were measured for thermal compared to TEOS oxides. The failure in both the TaN/thermal oxide and TaN/TEOS oxide systems was along the barrier/oxide interface. This discrepancy in adhesive properties may be rationalized in terms of the

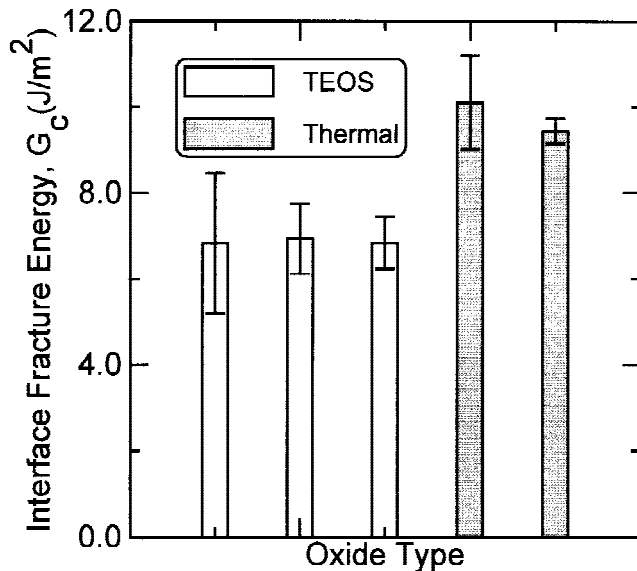


FIG. 9. Adhesion values for TaN on different oxides.

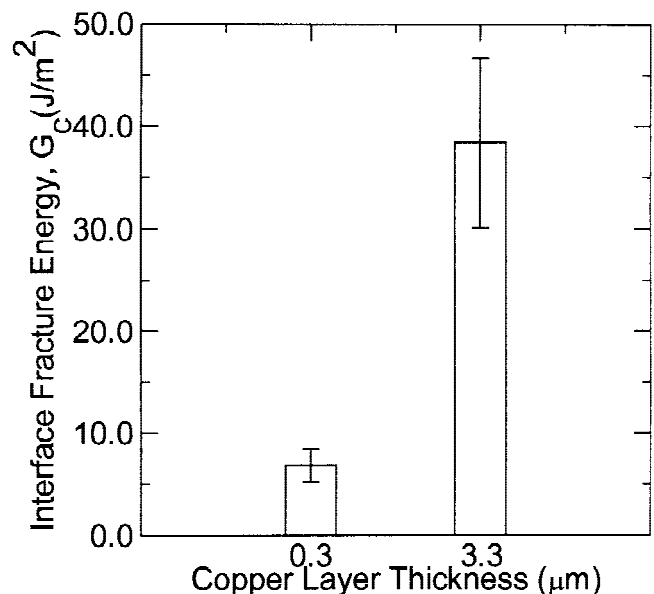
fracture properties of the oxides themselves and/or chemistry of the barrier/oxide interface. Segregation to the interface may reduce the intrinsic work of fracture according to<sup>24</sup>

$$G_o = W_{ad} - \sum(\Delta g_i^o - \Delta g_s^o)c_i \quad (6)$$

where  $c_i$  is the concentration of segregant per unit area of interface and  $\Delta g_i^o$  and  $\Delta g_s^o$  are the Gibbs free energy of the interface and segregant, respectively. The segregant may be in the form of either the carbon precursor to the silica film or moisture trapped in the glass which would lead to hydrolytic weakening of the interface.<sup>17</sup> In addition, the fracture properties of the oxides may be different. Fully dense thermal oxides are expected to be more fracture resistant than less dense TEOS oxides which contain residual polymer precursors. Particularly, debonds extending along an interface may seek out pores in the SiO<sub>2</sub> film and lower the macroscopic work of fracture more than that predicted by a rule of mixtures. While further studies are needed to more fully address this issue, it clearly underlies the need to carefully examine all films of the bimaterial couple and indicates that new silica deposition techniques must be carefully studied to ensure that adequate adhesion is maintained at interfaces.

Plastic dissipation in surrounding ductile layers has also been shown to have a large effect on the interface debond energy of multilayer interconnect structures.<sup>9–11</sup> Specifically, increasing plastic deformation was found to increase interface debond energies by >300% in aluminum interconnects and drive the debond path from the TiN/SiO<sub>2</sub> interface into the SiO<sub>2</sub>. These results have been modeled with both a mechanics of materials approach [embedded process zone (EPZ)], in which a zone

near the crack tip experiences very large strains and includes the rupture process<sup>26</sup> and a computational finite-element (FEM) analysis utilizing a virtual internal bond (VIB) rupture process.<sup>25</sup> Both models have been found to adequately predict the increase in interface fracture energy with increasing Al–Cu layer thickness. Similar results might be expected in copper interconnects although the extent to which plastic dissipation increases interface debond energy will vary due to differences in yield properties of Al and Cu thin films. Preliminary data showing interface fracture energy as a function of copper layer thickness is shown in Fig. 10. The interface fracture energy was increased by >400% as the copper layer thickness was increased from 0.3 to 3.3  $\mu\text{m}$ . On the basis of modeling results of the aforementioned Al–Cu interconnects,<sup>26</sup> estimates for increases in adhesion with Cu layer thickness may be made. Particularly, for a copper yield stress of 180 MPa and a work of adhesion of 4 J/m<sup>2</sup>, the relevant modeling length parameter, which scales with the plastic zone size, is found to be  $\sim 3.1 \mu\text{m}$ . Estimates based on predictions of the EPZ model suggest that a  $G_c$  of  $\sim 12$  times the work of adhesion ( $G_o$ ) or 48 J/m<sup>2</sup> should be anticipated for the copper thickness examined. FEM-based computational approaches provide similar estimates.<sup>27</sup> However, a number of parameters in these models, particularly the yield properties of the Cu layer and the value of  $G_o$ , still have a degree of uncertainty and must be more fully addressed through direct experimental measurements. Current work is underway to clarify these issues and measure adhesion values for a wide range of Cu layer thicknesses with detailed modeling of the plastic dissipation.

FIG. 10. Results showing the effect of copper layer thickness on the adhesion of the TaN/SiO<sub>2</sub> interface.

#### IV. CONCLUSIONS

The interface fracture energies of two important barrier/dielectric layers were investigated. The TaN/SiO<sub>2</sub> interface was found to have approximately twice the adhesion as the Ta/SiO<sub>2</sub> interface, and failure in both cases was along the barrier/SiO<sub>2</sub> interface rather than the barrier/copper interface. Furthermore, subcritical debonding data show that the TaN/SiO<sub>2</sub> interface is more resistant to time-dependent debonding than the Ta/SiO<sub>2</sub> interface. For samples produced with an initial 20 Å Ta layer, increasing the N content adjacent to the Ta(N)/SiO<sub>2</sub> interface in the TaN/Ta(N)/SiO<sub>2</sub> system was shown to have a dramatic effect on critical adhesion values. Evidence suggests that Ta<sub>2</sub>O<sub>5</sub> and Ta<sub>2</sub>Si reaction products at the interface together with the diffusion of N into the SiO<sub>2</sub> layer results in a more fracture resistant structure. Effects of dielectric type and Cu layer thickness were also investigated and are shown to have a significant effect on adhesion. Broader implications are that device reliability and yield may be significantly increased by careful consideration of the chemistry at the barrier/dielectric interface, the type of dielectric oxide, and the thickness of the metallization layer.

#### ACKNOWLEDGMENTS

This work was supported by the Director, Office of Energy Research, Office of Basic Energy Sciences, Materials Science Division of the United States Department of Energy, under Contract No. DE-FG03-95ER45543, and by the INTEL and Applied Materials Corps. M.L. was supported in part by an Intel Foundation Fellowship.

#### REFERENCES

1. S.P. Murarka and S.W. Hymes, *Crit. Rev. Solid State Mater. Sci.* **20**(2), 87 (1995).
2. C-S. Ryu, A.L.S. Loke, T. Nogami, and S.S. Wong, *Proc. IEEE-IRPS 201* (1997).
3. E.M. Zielinski, R.P. Vinci, and J.C. Bravman, *J. Electron. Mater.* **24**, 1485 (1995).
4. L. Stolt and F.M. d'Heurle, *Thin Solid Films* **189**, 269 (1990).
5. A. Cros, M.O. Aboelfotoh, and K.N. Tu, *J. Appl. Phys.* **67**, 3328 (1990).
6. E. Kolawa, J.S. Chen, J.S. Reid, P.J. Pokela, and M-A. Nicolet, *J. Appl. Phys.* **70**, 1369 (1991).
7. K. Holloway and P. Fryer, *Appl. Phys. Lett.* **57**, 1736 (1990).
8. J.W. Hutchinson and Z. Suo, in *Advances in Applied Mechanics*, edited by J.W. Hutchinson and T.Y. Yu (Academic Press, New York, 1991), pp. 63–191.
9. M. Lane, R.H. Dauskardt, R. Ware, Q. Ma, and H. Fujimoto, in *Materials Reliability in Microelectronics VII*, edited by J.J. Clement, R.R. Keller, K.S. Krisch, J.E. Sanchez, Jr., and Z. Zuo (*Mater. Res. Soc. Symp. Proc.* **473**, Pittsburgh, PA, 1997), pp. 21–26.
10. Q. Ma, J. Bumgarner, H. Fujimoto, M. Lane, and R.H. Dauskardt, in *Materials Reliability in Microelectronics VII*, edited by J.J. Clement, R.R. Keller, K.S. Krisch, J.E. Sanchez, Jr., and Z. Zuo (*Mater. Res. Soc. Symp. Proc.* **473**, Pittsburgh, PA, 1997), pp. 3–14.
11. R.H. Dauskardt, M. Lane, Q. Ma, and N. Krishna, *Eng. Fract. Mech.* **61**, 141 (1998).
12. M. Lane, R.H. Dauskardt, Q. Ma, H. Fujimoto, and N. Krishna, in *Thin-Films—Stresses and Mechanical Properties VII*, edited by R.C. Cammarata, M.A. Nastasi, E.P. Busso, and W.C. Oliver (*Mater. Res. Soc. Symp. Proc.* **505**, Warrendale, PA, 1998), pp. 357–362.
13. A.G. Evans, and J.W. Hutchinson, *Acta Metall.* **37**, 909 (1989).
14. A.G. Evans, M. Ruhle, B.J. Dalgleish, and P.G. Charalambides, *Metall. Trans. A* **21A**, 2419 (1990).
15. P. Gumbsh, *Mater. Sci. Eng.* **A260**, 72 (1999).
16. Q. Ma, *J. Mater. Res.* **12**, 840 (1997).
17. G. Xu, M-Y. He, and D.R. Clarke, *Acta Metall.* (1999, in press).
18. S.M. Wiederhorn, *J. Am. Ceram. Soc.* **50**, 407 (1967).
19. T. Michalske and B. Bunker, *J. Am. Ceram. Soc.* **70**, 780 (1987).
20. M. Lane and R.H. Dauskardt (unpublished).
21. A. Bhatnagar, M.J. Hoffman, and R.H. Dauskardt, *Am. Ceram. Soc.* (1999, in press).
22. J. Mencik, *Strength and Fracture of Glass and Ceramics* (Elsevier Science Publishers, New York, 1992).
23. *Handbook of Chemistry and Physics*, 72nd ed., edited by D. Lide (CRC Press, Boca Raton, FL, 1992).
24. J.R. Rice and J.S. Wang, *Mater. Sci. Eng.* **A107**, 23 (1989).
25. P. Klein and H. Gao, *Eng. Fract. Mech.* (1999, in press).
26. J.W. Hutchinson and A.G. Evans, Harvard University Report, May 1999.
27. M. Lane, A. Vainchtein, H. Gao and R.H. Dauskardt, Stanford University (1999, unpublished results).
28. C.D. Wagner and D.M. Bickham, *NIST X-ray Photoelectron Spectroscopy Database* (U.S. Department of Commerce, Washington, DC, 1989).